



Research Article

Numerical assessment of stability behaviour in supercritical CO₂ based NCLS configured with heater, heat exchanger and isothermal wall as heat sources

Srivatsa THIMMAIAH¹, Tabish WAHIDI^{1,*}, Ajay Kumar YADAV¹, Arun MAHALINGAM¹

¹Department of Mechanical Engineering, National Institute of Technology Karnataka, Surathkal, 620015, India

ARTICLE INFO

Article history

Received: 06 June 2021

Accepted: 01 October 2021

Keywords:

Supercritical CO₂; Instability;
Rectangular Natural Circulation
Loop; Flow Transition;
Computational Fluid Dynamics

ABSTRACT

Three-dimensional numerical analysis is presented in this study to assess the transient and stability behaviour of supercritical CO₂ (sCO₂) based NCLS configured with three different types of heat sources, i.e., heater, a hot heat exchanger (HHX) and isothermal wall (ISO) at the source, and a cold heat exchanger (CHX) at the sink in all three NCLS. Unsteady three-dimensional conservation equations (mass, momentum and energy equations) are solved to assess the transient and stability behaviour of sCO₂ mass flow rate, temperature and velocity as a function of time. Further, the effect of pressure on sCO₂ mass flow rate is also assessed to compare the loops performance. Performance of the loop has been studied for various heat inputs at the source by keeping constant mass flow rate and temperature at the sink. It is observed that for any boundary condition at the source, the loop experiences some initial disturbances or instabilities before reaching the steady-state. However, the time needed to attain a steady-state varies with the nature of heat input employed at the source. Results show a higher magnitude of instabilities in the Heater-CHX loop than HHX-CHX and ISO-CHX loops, and these instabilities mitigate at a faster rate in the ISO-CHX loop at all levels of heat input and operating pressure of the loop. It is also observed that as loop fluid operating pressure increases, the instability of the system decreases and the loop fluid mass flow rate increases. Further, the Nusselt number in the Heater-CHX loop is more than other loops because of its high turbulent kinetic energy. The findings of this study are validated with the published experimental and numerical data and found a good agreement.

Cite this article as: Srivatsa T, Tabish W, Ajay K Y, Arun M. Numerical assessment of stability behaviour in supercritical CO₂ based NCLS configured with heater, heat exchanger and isothermal wall as heat sources. J Ther Eng 2023;9(2):530–550.

*Corresponding author.

*E-mail address: tabishwahidi@gmail.com

This paper was recommended for publication in revised form by Regional Editor

Ahmet Selim



INTRODUCTION

Natural circulation loop (NCL) is one of the most promising and dominant mechanisms used to transport heat energy from a source to a sink. The driving force in NCL is developed by a thermally generated density gradient, which is generally accredited as buoyancy force. For the flow to get established in the loop, the buoyancy force shall be more significant than all the resistive forces encountered in the system. As the active elements like the pump or compressor are absent in the NCL, the buoyancy force alone has to surpass all the resistive forces in the loop. This inherent feature of NCL makes its operation more reliable in terms of safety than the forced circulation system. In NCLs, the balance shall accomplish between these two forces to bring a steady-state condition in the system. However, it is challenging to ensure a balance between these forces throughout the operation of the system and hence very often, and the loop has to experience indefinite oscillations. NCLs are highly economical in operation and maintenance due to the non-existence of active elements in the system and its constructional simplicity. NCLs techniques are incorporated in various applications like solar heaters, advanced nuclear reactor core cooling, geothermal energy extraction, blades cooling in a gas turbine, electronic components cooling etc., [1]. Notwithstanding all these applications and their popularity, the main drawback of NCLs is its very low Reynolds number, due to which the heat transfer rate in the system becomes low compared to the forced circulation loop [2]. Various researchers tried to explore the basic principles involved in the NCLs by using innumerable tools available and evolved with unprecedented concepts. In this direction, Mertol et al. [3] presented the distribution of pressure, temperature and velocity in NCL under laminar flow conditions by determining the variation of the friction and heat-transfer coefficients. The study of Lifshitz et al. [4] shows that the fluid flow characteristics in the NCLs depend on the initial conditions and the location of the state in the loop. Acosta et al. [5] observed maximum fluid velocity in single-phase NCL when it is kept at near zero-degree tilt angle, i.e., in a vertical position and the fluid velocity decreases with the loop tilt angle. The effects of wall thermal conductivity and wall thickness on heat transfer characteristics of a single-phase NCL is numerically investigated by Lin et al. [6] and found the existence of axial conduction through the thick and highly conductive wall of the loop, which tends to appreciably improve the buoyancy-induced circulating flow in the loop at lower modified Rayleigh number. One-dimensional mathematical model study of Cheng et al. [7] shows that an increase in loop diameter and temperature difference across the loop increases the steady-state Reynolds number; however, the modified Grashoff number and the heat transfer rate increase when temperature difference across the loop increases. Vijayan et al. [8] assessed various void fractions

and pressure drop correlations to predict the performance of NCLs.

CO₂ is a very few naturally available non-toxic and non-flammable working fluids that do not contribute to ozone depletion if it leaks to the atmosphere. It has very low global warming potential (GWP) (GWP~1) compared to synthetic refrigerants (GWP~1000). Hence CO₂ can easily and safely supersede all conventional working fluids like CFCs, HCFCs, hydrocarbons and ammonia in several fields of application. These environmentally benevolent nature and splendid thermo-physical properties of CO₂ made it gain more popularity as a primary and secondary working fluid in both natural and forced circulation systems. Yadav et al. [9] conducted a comparative analysis between CO₂ and other working fluids in forced circulation-type secondary loops. They concluded that it possesses an exceptional secondary fluid characteristic, which is very much required for refrigeration and air conditioning applications. For low-temperature refrigeration and air-conditioning applications, CO₂ based NCLs are very compact compared to other widespread conventional working fluids. The CO₂-based systems are used in various applications like high-quality copper and nickel extraction process by using sCO₂ solution along with hydrogen [10]. The operating pressure of sCO₂ based solar heater can be reduced by properly mixing it with Dimethyl ether, and this enhances the solar-thermal conversion efficiency and mass flow rate [11]. CO₂-based natural convection is an important design feature in the heat removal processes of advanced reactor designs [12]. By expanding liquid CO₂ in an expansion valve, solid-gas two-phase flows can be established, and cryogenic refrigeration can be achieved [13]. By employing sCO₂ as a refrigerant in refrigeration and air-conditioning applications, maximum heat transfer coefficient can be achieved at lower cooling pressure in the gas cooler [14]. CO₂ based heat pump water heater has a significant advantage over conventional heaters, wherein water temperature can be increased up to 90°C without any operational difficulties [15]. Pharmaceutical hydrates demonstrated very high solubility in sCO₂ compared to other anhydrous phases [16]. Despite its simplicity and compactness, a sCO₂ Rankine cycle can achieve high efficiency compared to a steam Rankine cycle if incorporated in the waste heat recovery system of a gas turbine [17].

CO₂ attains a supercritical fluid state when it operates above the temperature of 304.25 K and pressure of 7.37 MPa. The CO₂ system offers unique advantages when operated near or above the critical state compared to other fluids. The thermal physical properties of supercritical CO₂ vary greatly even when there is a small temperature change, as shown in Fig.1. Supercritical CO₂ possesses very low viscosity and a very high thermal expansion coefficient compared to other conventional working fluids. The three-dimensional CFD research results of Yadav et al. [18] reveal that the liquid CO₂ exhibits a seven times higher

heat transfer rate than water for the same wall temperature and geometrical parameters. Further, a similar rate of heat transfer is noticed when CO_2 is operated at near pseudo-critical region. In another 3-D CFD analysis of NCLs, Yadav et al. [19] noticed that near pseudo critical region, the heat transfer rate is much higher in the supercritical phase than the subcritical phase, however, for the subcritical phase, a higher heat transfer rate is noticed near-saturated liquid state. Thippeswamy and Yadav [20] compared the heat transfer performance of various conventional working fluids of NCL experimentally, like water and brine solution, with the subcritical and sCO_2 at various loop fluid operating pressure at various inlet temperatures to source & sink. It was observed that the heat transfer rates in the case of subcritical vapour, subcritical liquid, two-phase and sCO_2 based NCL are several times (4 to 9 times) higher than the water and brine-based NCLs. Hahne et al. [21] studied the natural convection heat transfer of sCO_2 and obtained maximum thermal conductivity in the vicinity of pseudocritical temperatures/pressures, and it is more pronounced as the critical point is approached.

Computational simulations of Zhang et al. [22] on the sCO_2 based NCLs show that higher Reynolds number mass flow can be established with sCO_2 as a working fluid, even for a small temperature difference (~ 8 K) between source and sink. Misale et al. [23] studied the influence of thermal capacity on the NCL behaviour and noticed that the Reynolds number increases if the wall thermal capacity decreases. At the supercritical region, the Nusselt number is found to have larger values than the near-critical and subcritical regions for CO_2 . In the supercritical region, time to reach steady-state also increases with increasing temperature and pressure values [24]. Chen et al. [25] numerically studied the effect of pipe diameter on the heat transfer and stability of sCO_2 based natural convective circulation system and found stabilized flow in a larger pipe diameter due to enhanced heat transfer and fully developed flow field. High-temperature sCO_2 based NCL study results of Sadhu et al. [26] show that the circulation rate can be maximized by increasing either the diameter and/or the loop height however, the performance of NCL with larger diameter tubes is better compared to loop with longer heights. Liu et al. [27] experimentally investigated the sCO_2 based NCL and noticed that the heat transfer coefficient decreases with increased heat flux and pressure. Deng et al.'s numerical and experimental results [28] on sCO_2 based NCL show that the mass flow will be susceptible to any change in input heat flux at the source. The experimental results of Yadav et al. [29] show that as the operating pressure of the sCO_2 increases, the time duration required to reach a steady-state of the system decreases. Numerical and experimental study by Yadav et al. [29-30] noticed that loop fluid mass flow rate decreases with a change in tilt angle. However, the heat transfer rate increases with an increase in external water mass flow rate and hot water inlet temperature but decreases

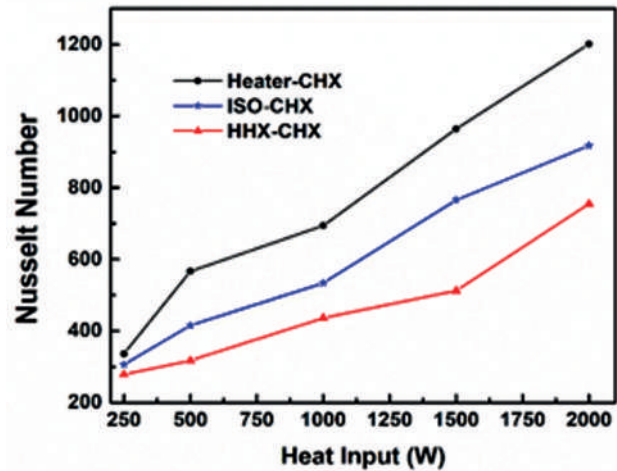


Figure 1. Thermophysical property variations of CO_2 at 90 bar.

with a change in tilt angle. Further, the loop was found to be stable under the pulsating mass flow rate of external hot and cold water. CFD analysis of Archana et al. [31] on sCO_2 based NCL reveals that as the loop fluid pressure increases, the heat transfer coefficient decreases from its peak value, whereas steady-state mass flow rate increases. Karakurt et al. [32] provide a reference for finding optimal operating conditions and the design parameters for real sCO_2 Brayton power cycles. Wang et al. [33] did a performance and flow distribution of the plate heat exchanger with supercritical carbon dioxide fluid and found higher efficiency and pressure is evenly distributed sCO_2 compared to water.

Due to the nonlinearity of the natural convection process, any disturbance in the driving force causes the disturbance in the flow and leads to oscillatory behaviour even when an eventual steady-state is expected. Therefore, NCLs always require a precise assessment to time that focuses on the flow behaviour and the actual thermo-physical phenomenon happening in the NCL. The flow and temperature fields in the NCLs are inter-dependent, and hence it is not possible to have direct control over the circulation rate or direction of flow/circulation in the loop, this inherent nature of NCL propels the loop into instability. The small driving force, i.e., buoyancy force and its nonlinear nature of the natural convection, intrinsically make the NCLs more unstable than the forced circulation system. It is essential to comprehend the characteristics of NCL stability before integrating it into any practical applications. The mass flow stability can be categorized as neutral if the mass flow rate oscillates with a smaller amplitude and the flow velocity remains in the same direction, and similarly, it can be categorized as unstable if the oscillations keep growing with time and lead to flow reversal. Chen et al. [34] carried out an analytical and numerical investigation to study the

flow instability in single-phase thermosyphons over a range of loop aspect ratios and expressed the steady-state results in terms of a single dimensionless parameter. When this parameter is less than a critical value, the flow is stable, and above this value, the flow is unstable. Further, it is observed that when the aspect ratio of the loop approaches unity, the flow is least stable. In the supercritical region, the loop experiences mass flow rate instability due to sharp changes in the density of loop fluid near pseudo-critical points. Flow instability at the supercritical state is highly unacceptable as it can induct harmful mechanical vibration in the system components, and eventually it may lead to catastrophic incidences due to fatigue development in the components. Further, if oscillations get augmented, it can affect the heat transfer characteristics, which will be detrimental to the system efficiency. Many investigators profoundly studied the natural circulation system to comprehend the nature of instability, and some of the observations of a few researchers are given below.

In a one-Dimensional rectangular-shaped model, Keller first observed and reported a periodic oscillatory motion of the loop fluid [35] when certain parameter in loop exceeds certain limits and concluded that these oscillations depend on the interaction between frictional and buoyancy forces but not on inertial force. In a theoretical discussion, Welander [36] mentioned that the solution of differentially heated loop fluid is susceptible to instability in an oscillatory manner, i.e., a weaker instability will be in the form of pulsations with a unidirectional motion, while a stronger instability will be bidirectional and also these oscillations are found to be irregular. Schuster et al. [37] investigated the thermo-hydraulic properties of integrated reactor concepts with a natural circulation driven primary loop and concluded that it is not possible to reach a stable two-phase flow in the loop without passing through flow instabilities. Further, at heating and cooling power equilibrium, the flow oscillations can exist at nearly constant frequencies and amplitudes. A one-Dimensional steady-state NCL stability analysis by Vijayan et al. [38] shows that the flow rate gets enhanced with an increase in loop diameter for all three regions. Significant influence of pressure is noticed on the flow rate and stability of the system in the two-phase region. In a toroidal thermosyphon, at steady-state regime, Stern et al. [39] measured the fluid temperature across the heating section for a range of heat fluxes and reported that in all the cases, the highest temperature occurred at the inner wall location and the greatest amplitudes of the fluctuations occurred at the locations near, but not at the inner walls. Chen et al. [40] carried out numerical simulations to investigate flow transitions and instabilities in a sCO₂ based NCL and found that at specific heat source temperature, i.e., at around 375 K, which is near the second pseudo-critical temperature, the loop fluid in the system changes from unstable bidirectional flow into a stable unidirectional flow as the fluid properties experience major

transitions. The experimental observation of Creveling et al. [41] on single-phase free convection loop shows that at higher and lower heat-transfer rates, the loop fluid flow was steady but highly oscillatory at intermediate ranges of heat-transfer. An experimental study by Kapitz et al. [42] showed that the nucleation sites in the NCLs will strongly impact stability behaviour, especially for low heat flux levels. Misale et al. [43] experimentally studied the behaviour of a single-phase NCL to analyze the influence of constant/variable power input at the source and observed temperature oscillations in both cases. However, an increase in amplitude and frequency of these oscillations was noticed with an increase in power input. Furuya et al. [44] experimentally investigated the effect of inlet restriction on thermal-hydraulic stability. Results show that the driving force of the natural circulation at the stability boundary is a function of heat flux and inlet sub-cooling but independent of inlet restriction.

Over time, numerous researchers have developed plenty of solutions techniques to tackle or at least mitigate the instability issue in the NCLs; however, this enigma is yet to be resolved completely. The following section is attributed to the consummate contribution of such researchers to the NCL turf. Yadav et al. [45] developed a 3-D CFD model for both subcritical and sCO₂ based NCLs to study the effect of loop tilting in different planes and concluded that by changing the orientation of the loop, the flow instability issues in the NCLs can be tackled, but it will deteriorate the heat transfer rate. Manero et al. [46] observed that in the two-phase NCLs, during bubble boiling, the oscillation frequency is inversely proportional to a single vapour bubble formation and breaking cut-off time. For a small inclination of the loop, the frequency of oscillation of temperature and pressure is higher as the time of formation and breaking of a single bubble is smaller, however for larger inclinations, the time required for the same is larger, and thus the frequency of oscillation of temperature and pressure is lower. In a 3-D steady flow simulation of a CO₂ based NCL, Yadav et al. [47] developed a new-correlations between Reynolds Number and friction factor, and these correlations are helpful in the design and analysis of NCLs with end heat exchangers. Zvirin [48] analytically investigated the effects of through-flow on the flow rates and temperature distributions in a NCL at various loop parameters by employing a one-dimensional spatial model and found that the through-flow stabilizes the motion in the loop. Cammarata et al. [49] experimentally examined the effect of change in gravity and thermal boundary conditions on the dynamics of NCLs. They concluded that the dynamics of NCL stabilizes with the reduced gravitational field, but it enhances the thermal stresses on the system. In another breakthrough, Cammarata et al. [50] developed a control strategy by employing standard P.I.D (proportional integral derivative) control to counteract instabilities in NCL, and it is

found to be suitable for avoiding the flow inversion of the working fluid inside the NCL. Jiang et al. [51] conducted a 3-D nonlinear model study on NCL by incorporating the flow modes and proposed an algorithm to control the flow instability by varying the thermal boundary condition. Vijayan et al. noticed that when the heater and the cooler are orientated horizontally, the mass flow was found to be at its peak at a specified operating condition, but the system was least stable. However, with a vertically orientated heater and cooler, the system was found to be most stable. Chen et al. [53] carried out numerical simulations to investigate the influence of heater orientations on the performance of $s\text{CO}_2$ based NCLs. A vertically orientated heater is found to be stable, whereas a horizontally orientated heater shown oscillatory behaviour. Further, the cooler heat transfer behaviour significantly affects the heat transfer and stability of the loop.

Bidirectional flow in NCLs is a very common phenomenon, and it adversely affects the heat transfer performance of the loop. To address the flow reversal issues in the NCLs, Wahidi et al. [54] carried out a two-dimensional CFD simulation by introducing a modified Tesla valve in the riser of a $s\text{CO}_2$ based NCL and achieved unidirectional fluid flow circulation in the loop. Further, with the Tesla valve in NCLs, the velocity and temperature oscillations were also found substantially mitigated without reducing the heat transfer performance. In the process of combating the instability issues in NCLs, Wahidi and Yadav [55] incorporated tesla valve in both riser and downcomer of loop and found further mitigation of velocity and temperature oscillation but at the cost of 3% reduction in the heat transfer performance of the loop. Sharma et al. [56] developed computer codes to analyze the linear and nonlinear stability behaviour of supercritical water in the natural circulation loop and developed the stability maps. Seyyedi et al. [57] numerically studied a simple rectangular single-phase NCL and developed a stability map valid for all three flow regions. Manthey et al. [58] experimentally studied the influence of the flow resistance on the two-phase flow stability and their oscillatory behaviour in an open natural circulation system and summarized its variation in stability maps. Jiang et al. [59] analyzed the static and dynamic behaviour of NCL and developed an instability map of the system, and distinctly marked its various regions. Rao et al. [60] studied the transient stability behaviour of NCL using the finite element program and constructed the stability envelope.

NCLs can be configured with various heat source and heat sink combinations depending on the application requirement and the available resources to transport heat energy from higher to lower energy levels. Natural circulation loops incorporated with various mechanisms of heat addition and rejection at source and sink, respectively, show different instability types. It is mandatory to comprehend the dynamic behaviour of each of these combinations

before implementing it in a particular application. In view of this, Thimmaiah et al. [61] carried out 2-D CFD analysis on two different configurations of $s\text{CO}_2$ based NCLs, i.e., NCL with isothermal wall and a cold heat-exchanger, and NCL with hot and cold heat-exchangers to compare the dynamic performance and results show the higher instabilities in both side heat-exchanger loop than an isothermal wall with heat-exchanger loop.

As discussed above, extensive study and research have been carried out on the stability analysis of different types of NCLs considering different geometrical designs (toroidal, rectangular loops etc.), different working fluids (water, brine solution, CO_2 etc.), a different state of working fluid (Subcritical and supercritical state) etc., by various researchers. However, no literature is available on the 3-D numerical comparative study of oscillatory instability of supercritical CO_2 with different geometries and boundary conditions. In this research, the focus is on transient 3-D numerical analysis of $s\text{CO}_2$, loop fluid, in NCLs configured with various kinds of heat inputs at the source of the NCL like Heater, a Heat exchanger (HHX) and Isothermal wall (ISO), and cold heat exchanger at the sink (CHX) by changing the intensity of heat input at source and operating pressure of the loop fluid.

PHYSICAL MODEL OF NCL

Comparative analysis has been conducted between three different $s\text{CO}_2$ based NCLs, i.e., one configured with Heater-CHX loop (Fig. 2a), the second one configured with HHX-CHX loop (Fig. 2b) and the third one with ISO-CHX loop (Fig. 2c). In these loops, the effect of heat input on the mass flow rate, temperature and velocity of the loop fluid ($s\text{CO}_2$) have been studied along with the effect of pressure on the mass flow rate. For all the NCLs, the magnitude of heat input at the source varied for all the operating pressure of the loop fluid, which is varied from 80 to 100 bar in a step of 10bar. For all the operating pressure and heat input cases, the loop sink temperature, i.e., CHX inlet temperature, has been kept constant at 305 K. Both the right and left legs are assumed to be adiabatic. The Loops are kept in a vertical plane to ensure the maximum mass flow rate of loop fluid [52]. All the geometrical and material specifications of the model are given in Table 1.

Figure 2 shows a rectangular NCL schematic consisting of a heating source, a left leg, a cold heat-exchanger (CHX), and a right leg. The loop fluid is heated from below at the heater with constant heat inputs and is cooled sensibly by rejecting heat to the external fluid (water) in the CHX. Circulation of the loop fluid is maintained due to the buoyancy effect caused by heating at the bottom and cooling at the top. Water is used as a coolant at a heat-exchanger at a fixed mass flow rate (0.1 kg/s) to ensure the turbulent flow. At the isothermal wall, constant temperature is imposed.

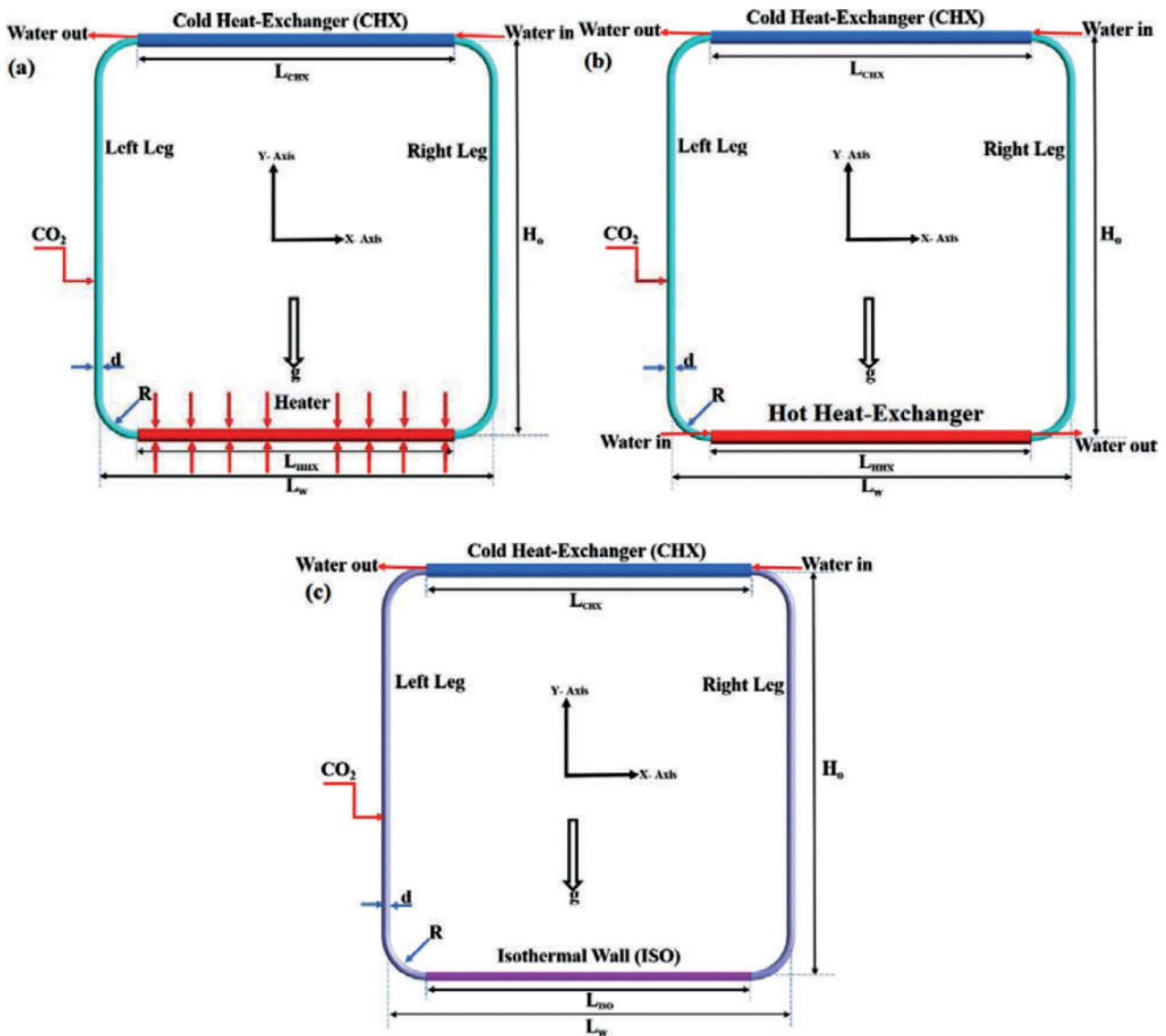


Figure 2. Schematic of natural circulation loop.

Table 1. Geometrical specification of loop used in the present study

Parameter	Value
Inner tube diameter	10 mm
Outer tube diameter	16 mm
Length of heat exchangers (L)	400 mm
Length of heater (L)	400 mm
Length of Isothermal wall (L)	400 mm
Height of the loop (H_0)	500 mm
Width of the loop	500 mm
Diameter of the loop (d)	10 mm
Curvature radius of the bend (R)	50 mm
Total length of the loop (L_t)	1914mm
Material of the loop	Stainless steel

GRID INDEPENDENCE STUDY

Grid independence study conducted at 1500 W of heat input at source for Heater-CHX loop and the same quantum of heat input, the evaluated corresponding temperature at the inlet of HHX-CHX loop is 317.5 K and similarly at Isothermal wall of ISO-CHX loop is 311.5 K. The loop fluid operating pressure is kept at 90 bar, and constant temperature of 305 K is maintained at the inlet of CHX of all the loops. The geometrical model considered for 3-dimensional CFD simulation of NCLs comprises loop fluid (sCO_2) in the loop primary side of the fluid region, a wall thickness of the pipe and cooling fluid (water) in the secondary side of the fluid region, i.e., in the cold heat exchanger.

A sensitivity analysis has been carried out in the modelled grid to study the grid independence to obtain the solution independent from the adopted grid and time. Initially,

coarse meshing is framed and progressively refined until an independent mesh result is obtained. For meshing the three-dimensional loop geometry, the design modeler of the ANSYS 19.0 software is employed. Figure 3 shows the cross-sectional view of the CHX, wherein meshing is carried out for the sCO₂ region, cooling water region and piping.

For the CO₂ region, in a radial direction close to the wall, grid sizing is kept as minimum as 0.25 mm and moving farther from the wall, it is increased to a maximum size of 1mm. Since the property variation is very minimal for water, a uniform grid sizing of 1 mm is envisaged in this region. In the axial direction, i.e., in horizontal pipes including bends, coarse meshing of grid size 1.0 mm is

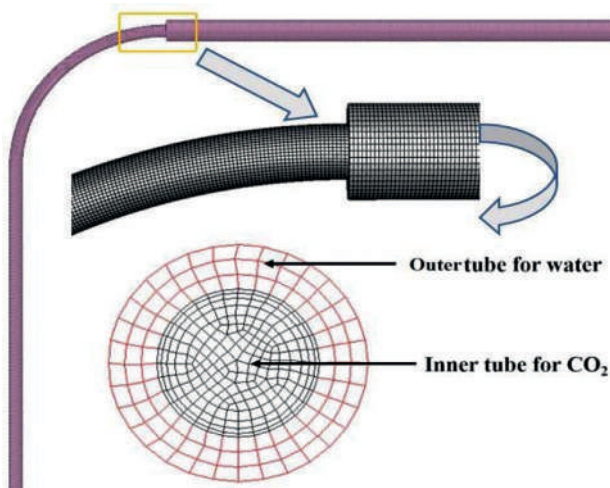


Figure 3: Mesh generated for the computational domain.

adopted and in vertical pipes 2.0 mm grid size is considered. With this mesh generation, a yield of total of 400,704 nodes is obtained. To deal with the turbulence models near-wall region is to use the wall functions. Wall functions are equations empirically derived and used to satisfy the physics in the near-wall region. The first cell centre needs to be placed in the log-law region to ensure the accuracy of the results. Wall functions are used to bridge the inner region between the wall and the turbulence fully developed region. When using the wall functions approach, there is no need to resolve the boundary layer causing a significant reduction of the mesh size and the computational domain. The first grid cell needs to be $30 < y^+ < 300$ (if this is too low, the model is invalid, if this is too high, the wall is not properly resolved). To ensure the optimal choice of fineness of the grid, a minimum value of 38.39 for Y+ value has been used with a standard wall function near the wall.

The grid-independence test is carried out to check the reliability of obtained results (as shown in Fig. 4a for Heater CHX & ISO-CHX loops and Fig. 4b for HHX-CHX loop). The grid convergence index (GCI) method proposed by Roache et al. [62] is utilized for performing the grid-independent study. GCI method is based on the application of Richardson’s extrapolation, in which the spatial and temporal (in unsteady numerical simulations) discretization errors approach to zero asymptotically as the grid is refined, i.e., grid cells become smaller and the number of cells in the flow domain increase. With the GCI method of Roache et al. [62], the estimated error is 1.6 % for the mesh generated using 400,704 nodes in the NCLs.

The time step independence study is also performed on the Heater-CHX loop for the mesh generated above, i.e., 400,704 nodes. For the heat input of 1000 W at source and loop fluid operating pressure of 90 bar, the flow initiation

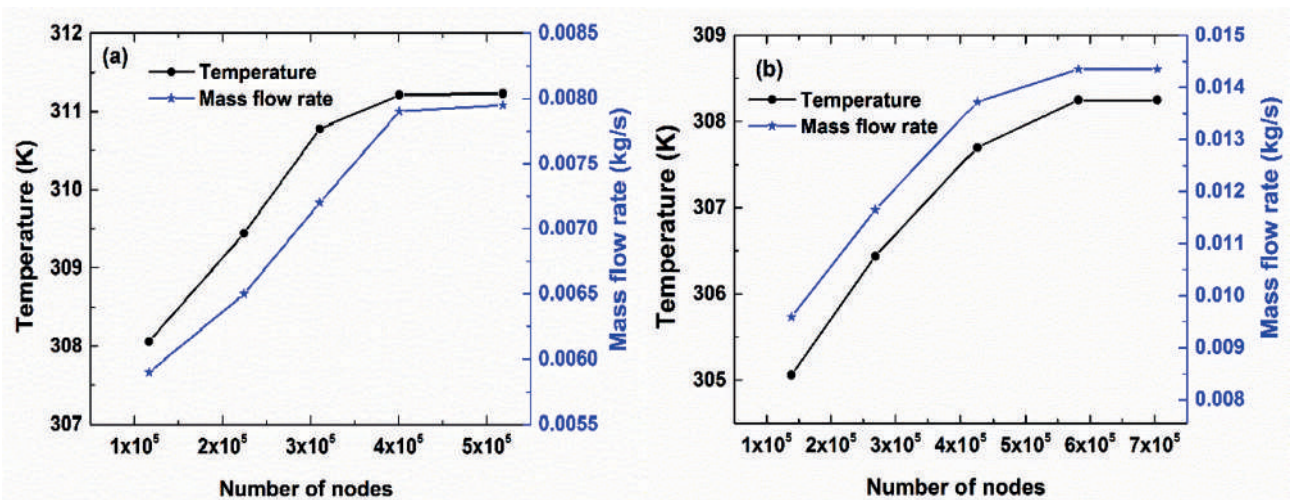


Figure 4. Grid independence study for supercritical CO₂ based natural circulation loop for (a) Heater-CHX and (b) HHX-CHX.

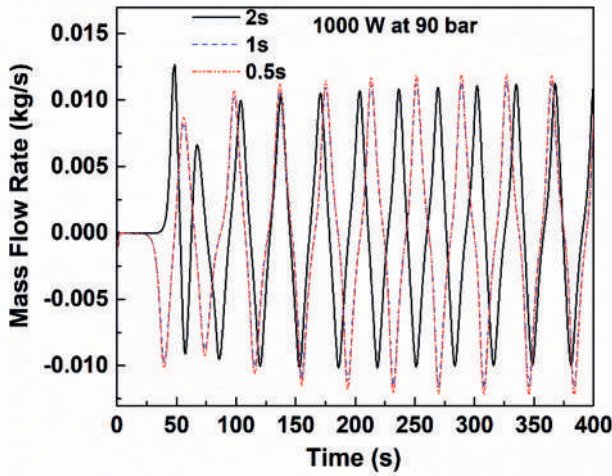


Figure 5. Time independent study for supercritical CO₂ based natural circulation loop at operating pressure of 100 bar for a heat input of 1000 W at different time steps.

transient in the model configuration was computed with time steps of 0.5 s, 1 s, and 2 s, and the result thus obtained is depicted in Fig. 5. It is evident from the graph that there is hardly any difference between results of 0.5 s and 1 s. Hence for employing better computational efficiency, the time step of 1 s is finally chosen.

MATHEMATICAL FORMULATION

The fundamental conservation equations (mass, momentum and energy) solved for the simulation are given below. The commercial software ANSYS (FLUENT) V-19.0 is employed to solve these equations with the associated boundary specifications.

The mass conservation equation can be given as:

$$\frac{\partial}{\partial t} \rho + \frac{\partial}{\partial x} \rho u + \frac{\partial}{\partial y} \rho v + \frac{\partial}{\partial z} \rho w = 0 \quad (1)$$

Momentum Conservation:

In X-direction

$$\begin{aligned} & \frac{\partial}{\partial t} \rho u + \frac{\partial}{\partial x} \left[\rho u u - \frac{4}{3} (\mu + \mu_T) \frac{\partial u}{\partial x} \right] + \frac{\partial}{\partial y} \left[\rho u v - (\mu + \mu_T) \frac{\partial u}{\partial y} \right] + \frac{\partial}{\partial z} \left[\rho u w - (\mu + \mu_T) \frac{\partial u}{\partial z} \right] \\ & = -\frac{\partial p}{\partial x} - \frac{2}{3} \mu \left[\frac{\partial v}{\partial y} + \frac{\partial w}{\partial z} \right] + \frac{\partial}{\partial y} \left[(\mu + \mu_T) \frac{\partial v}{\partial x} \right] \\ & + \frac{\partial}{\partial z} \left[(\mu + \mu_T) \frac{\partial w}{\partial x} \right] - \frac{2}{3} \frac{\partial}{\partial x} (\rho) \end{aligned} \quad (2)$$

In Y-direction

$$\begin{aligned} & \frac{\partial}{\partial t} \rho v + \frac{\partial}{\partial x} \left[\rho v u - (\mu + \mu_T) \frac{\partial v}{\partial x} \right] + \frac{\partial}{\partial y} \left[\rho v v - \frac{4}{3} (\mu + \mu_T) \frac{\partial v}{\partial y} \right] + \frac{\partial}{\partial z} \left[\rho v w - (\mu + \mu_T) \frac{\partial v}{\partial z} \right] \\ & = -\frac{\partial p}{\partial y} - \frac{2}{3} \mu \left[\frac{\partial u}{\partial x} + \frac{\partial w}{\partial z} \right] + \frac{\partial}{\partial x} \left[(\mu + \mu_T) \frac{\partial u}{\partial y} \right] \\ & + \frac{\partial}{\partial z} \left[(\mu + \mu_T) \frac{\partial w}{\partial y} \right] - \frac{2}{3} \frac{\partial}{\partial y} (\rho) - \rho g \end{aligned} \quad (3)$$

In Z-direction

$$\begin{aligned} & \frac{\partial}{\partial t} \rho w + \frac{\partial}{\partial x} \left[\rho w u - (\mu + \mu_T) \frac{\partial w}{\partial x} \right] + \frac{\partial}{\partial y} \left[\rho w v - (\mu + \mu_T) \frac{\partial w}{\partial y} \right] + \frac{\partial}{\partial z} \left[\rho w w - \frac{4}{3} (\mu + \mu_T) \frac{\partial w}{\partial z} \right] \\ & = -\frac{\partial p}{\partial z} - \frac{2}{3} \mu \left[\frac{\partial u}{\partial x} + \frac{\partial v}{\partial y} \right] + \frac{\partial}{\partial x} \left[(\mu + \mu_T) \frac{\partial u}{\partial z} \right] \\ & + \frac{\partial}{\partial y} \left[(\mu + \mu_T) \frac{\partial v}{\partial z} \right] - \frac{2}{3} \frac{\partial}{\partial z} (\rho) \end{aligned} \quad (4)$$

Energy equation is given as

$$\begin{aligned} & \frac{\partial}{\partial t} \rho h + \frac{\partial}{\partial x} \left[\rho h u - \frac{\mu_T}{Pr_T} \frac{\partial h}{\partial x} \right] + \frac{\partial}{\partial y} \left[\rho h v - \frac{\mu_T}{Pr_T} \frac{\partial h}{\partial y} \right] \\ & + \frac{\partial}{\partial z} \left[\rho h w - \frac{\mu_T}{Pr_T} \frac{\partial h}{\partial z} \right] = \frac{\partial p}{\partial t} + u \frac{\partial p}{\partial x} + v \frac{\partial p}{\partial y} + w \frac{\partial p}{\partial z} \\ & + \frac{\partial}{\partial x} \left(\lambda \frac{\partial T}{\partial x} \right) + \frac{\partial}{\partial y} \left(\lambda \frac{\partial T}{\partial y} \right) + \frac{\partial}{\partial z} \left(\lambda \frac{\partial T}{\partial z} \right) \end{aligned} \quad (5)$$

Turbulence Model

Turbulence models for supercritical fluids are in a developing stage. In previous studies, Chen et al. [25], Lisboa et al. [63], and Yadav et al. [18] have used the Renormalization Group (RNG) $k-\epsilon$ model for sCO₂-NCL and achieved accurate results.

Governing equations for the RNG $k-\epsilon$ model include two equations.

Turbulent kinetic energy equation

$$\begin{aligned} & \frac{\partial}{\partial t} \rho k + \frac{\partial}{\partial x} \left[\rho u k - \frac{\mu_T}{\sigma_k} \frac{\partial k}{\partial x} \right] + \frac{\partial}{\partial y} \left[\rho v k - \frac{\mu_T}{\sigma_k} \frac{\partial k}{\partial y} \right] \\ & + \frac{\partial}{\partial z} \left[\rho w k - \frac{\mu_T}{\sigma_k} \frac{\partial k}{\partial z} \right] = G - \rho \epsilon \end{aligned} \quad (6)$$

Where,

$$G = \mu_T \left(2 \left[\left(\frac{\partial u}{\partial x} \right)^2 + \left(\frac{\partial v}{\partial y} \right)^2 + \left(\frac{\partial w}{\partial z} \right)^2 \right] + \left(\frac{\partial u}{\partial y} + \frac{\partial v}{\partial x} \right)^2 + \left(\frac{\partial u}{\partial z} + \frac{\partial w}{\partial x} \right)^2 + \left(\frac{\partial v}{\partial z} + \frac{\partial w}{\partial y} \right)^2 \right) \quad (7)$$

Turbulent kinetic energy dissipation equation

$$\frac{\partial}{\partial t} \rho \varepsilon + \frac{\partial}{\partial x} \left(\rho u \varepsilon - \frac{\mu_T}{\sigma_\varepsilon} \frac{\partial \varepsilon}{\partial x} \right) + \frac{\partial}{\partial y} \left(\rho v \varepsilon - \frac{\mu_T}{\sigma_\varepsilon} \frac{\partial \varepsilon}{\partial y} \right) + \frac{\partial}{\partial z} \left(\rho w \varepsilon - \frac{\mu_T}{\sigma_\varepsilon} \frac{\partial \varepsilon}{\partial z} \right) = c_1 \frac{\varepsilon}{\kappa} G - c_2 \rho \frac{\varepsilon^2}{\kappa} - R \quad (8)$$

Where,

$$R = \frac{c_\mu \eta^3 \rho \left(1 - \frac{\eta}{\eta_0} \right) \varepsilon^2}{\kappa (1 + \beta \eta^3)} \quad (9)$$

$$\eta = \frac{S \kappa}{\varepsilon} \text{ and } S = \frac{1}{\sqrt{2}} \left(\frac{\partial u}{\partial y} + \frac{\partial u}{\partial z} + \frac{\partial v}{\partial x} + \frac{\partial v}{\partial z} + \frac{\partial w}{\partial x} + \frac{\partial w}{\partial y} \right) \quad (10)$$

Value of constants:

$$\eta_0 = 4.8, \beta = 0.012, c_\mu = 0.0845, \sigma_\varepsilon = \sigma_\kappa = 0.7178, c_1 = 1.42 \text{ and } c_2 = 1.68 \quad (11)$$

$$\mu_T = c_\mu \rho \frac{\kappa^2}{\varepsilon} \quad (12)$$

The following terms are defined to describe the fluid flow and heat transfer phenomena.

Mass flow rate at any cross-section is defined as,

$$\dot{m} = \int_0^A \rho_r \bar{V}_r \cdot dA' \quad (13)$$

The local flow velocity can be given as:

$$u_x = \frac{\int_0^A u_r |\rho_r \bar{V}_r \cdot dA|}{\int_0^A |\rho_r \bar{V}_r \cdot dA|} \quad (14)$$

Local temperature is given by,

$$T_x = \frac{\int_0^A T_r |\rho_r \bar{V}_r \cdot dA|}{\int_0^A |\rho_r \bar{V}_r \cdot dA|} \quad (15)$$

Modified Grashof number [29] are defined as follows:

$$Gr_m = \frac{g \beta d^3 \rho^2 Q H_0}{A \mu^3 C_p} \quad (16)$$

The local Nusselt number for heating or cooling wall is defined as:

$$Nu_x = \frac{h_x D}{\lambda_x} \quad (17)$$

The local heat transfer coefficient h_x is given by

$$h_x = \frac{q_x}{T_{wall} - T_{b,x}} \quad (18)$$

The heat flux q_x on the wall is defined as:

$$q_x = \lambda_x \left(\frac{\partial T}{\partial y} \right)_w \quad (19)$$

The Nusselt number of heat transfer wall is

$$Nu = \frac{\int_0^L Nu_x dx}{L} \quad (20)$$

All the properties are calculated at the bulk to mean temperature (T_m) of loop fluid, defined as:

$$T_m = \frac{\sum_{i=1}^n T_i}{n} \quad (21)$$

SIMULATION DETAIL

A three-dimensional transient simulation is performed for the geometries shown in Fig. 2 using ANSYS Fluent research version 19.0. Both right and left legs of a loop are considered to be perfectly insulated to ensure adiabatic condition. The wall thickness at the source and sink is considered as 3 mm for simulation. A Navier-Stokes equation, wherein the pressure-velocity are coupled, have been solved by using SIMPLE (Semi-Implicit Method for Pressure- Linked Equations) algorithm. The velocity and temperature parameters in the momentum and energy governing equations are iterated with a second-order upwind scheme. Similarly, the turbulence parameters (k-ε etc.) are also iterated with a second-order upwind scheme. The pressure term in the momentum equation is discretized by using PRESTO (Pressure staggering option). No-slip boundary condition is considered for pipe walls. A general Renormalization Group RNG k-ε model is used to account for turbulence in the loop fluid. Further, the axial conductivity and viscous dissipation in loop fluid are considered in the simulation. Convergence is achieved when residuals

of the all-governing equations are less than 10^{-3} except the energy equation, which was less than 10^{-6} . For simulation, the operating pressure of sCO_2 , i.e., loop fluid, was kept at 80, 90 and 100 bar to ensure it at the supercritical region. A NIST REFPROP property table [64] was utilized to obtain

all the standard properties of CO_2 for every interval of 2 K temperature & piecewise-linear interpolation was used to obtain property between two data points. While the following assumptions/boundary conditions are considered in the analysis is given in Table 2.

Table 2: Assumptions/boundary conditions are considered in the analysis

S. No.	Description
1	The internal (CO_2) and external (water) fluid are in single-phase throughout the loop.
2	Loop fluid is supercritical CO_2 (Pressure varies from 80 bar to 100 bar).
3	Left and right leg wall are assumed to be adiabatic.
4	No-slip condition near the wall.
5	Wall thickness is kept 3 mm.
6	CHX inlet water temperature is supplied at 305 K.

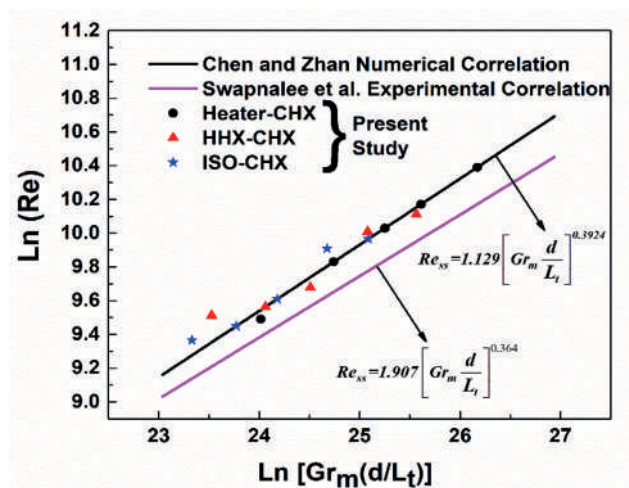


Figure 6. Validation of the obtained result with correlations $\ln(Re)$ and $\ln(Gr_m d/L_t)$.

VALIDATION

Obtained 3D CFD results are validated with a correlation of Reynolds Number and modified Grashof number, i.e., $Re-Gr_m$ in two different ways:

- i. Numerical correlation validation with $Re-Gr_m$ developed by Chen and Zhang [25].
- ii. Experimental correlations validation with $Re-Gr_m$ developed by Swapnalee et al. [65]

The correlations available in the literature have been selected to validate the obtained results, i.e., the numerical correlation developed by Chen and Zhang [25] and the experimental correlation developed by Swapnalee et al. [65]. These correlations relate to two non-dimensional parameters, i.e., Reynolds number (Re) and modified Grashof number ($Gr_m d/L_t$), calculated at the heating section of the loop. CFD simulation results obtained for 90 bar are validated using these correlations. Good agreement was found between the generated results and existing correlations, as shown in Fig. 6. The maximum discrepancies are less than 2% with the numerical correlation [25] and less than 6% with the experimental correlation [65].

Numerical Correlation by Chen and Zhang [25]

$$Re = 1.129 (Gr_m d / L_t)^{0.3924}$$

Experimental Correlation by Swapnalee et al. [65]

$$Re = 1.907 (Gr_m d / L_t)^{0.364}$$

RESULTS AND DISCUSSION

To compare the transient and instability behaviour of sCO_2 in square-natural circulation loops, a

Table 3: Heat fluxes imposed at the heater and its corresponding temperature derived at HHX and ISO

S. NO	Heat Input at Heater (W)	Corresponding temperature		
		Hot Heat Exchanger		Isothermal Wall
		Inlet to HHX	Outlet from HHX	
1	250	308.50	307.81	306.00
2	500	310.75	309.38	308.00
3	1000	314.25	311.50	309.75
4	1500	317.50	313.38	311.50
5	2000	320.75	315.25	313.50

three-dimensional CFD simulation is carried out for three different NCL loop configurations. These loops are subjected to the same quantum of heat at the source, but with varying boundary conditions, i.e., the first loop is exposed to the heater, the second loop is exposed to a hot heat exchanger, and the third loop to an Isothermal wall at their respective sources. The heating section of the Heater-CHX loop is exposed to 250 W, 500 W, 1000 W, 1500 W and 2000 W heat fluxes at various pressures, i.e., 80, 90 and 100 bar. Whereas an equal quantity of heat is injected to the HHX-CHX loop by circulating hot water of the corresponding temperature at the inlet of HHX. Similarly, corresponding constant temperature is maintained throughout the Isothermal wall of the ISO-CHX loop. The ISO-Wall temperature and HHX inlet/outlet temperature, corresponding to heat input at 250 W to 2000 W heat fluxes, is tabulated in Table 3. These values are derived from the steady-state condition of the Heater-CHX loop for the ISO-CHX loop and evaluated analytically for the HHX-CHX loop. Further, to maintain the similarity in the heat rejection process, all these three loops are configured with a cold heat exchanger at their respective sinks.

The heating section of loops receives the heat energy from three different kinds of boundary conditions, but the cooling section of all these loops rejects the heat through a cold heat exchanger, which is maintained at a constant temperature of 305 K at the inlet of the cooler. The heating section of the loop is exposed to the following three boundary conditions at the heat source.

- **Loop:1** Heater: Heat energy is transferred to the loop fluid by exposing the entire heating section of the loop to a constant heat flux.
- **Loop:2** Heat Exchanger: The loop fluid receives heat energy through a hot heat exchanger, wherein the intensity of heat input to the loop fluid depletes across the length of the heating section of the loop.
- **Loop:3** Isothermal heat addition: The loop fluid is exposed to a uniform temperature throughout the heating section of the loop.

The loops which are configured with the above three boundary conditions are depicted in Fig. 2. Further, in all the simulation cases, the initial temperature of the loop fluid at all the sections of the loop is kept at 305 K. The transient variation in loop fluid mass flow, temperature and velocity at various pressures and heat input along with the effect of pressure on mass flow rate have been recorded at the mid of left vertical leg and discussed in the following sections.

Transient variation of temperature

Figure 7 below shows the variation of loop fluid temperature in three differently configured NCLs, i.e., Heater-CHX, HHX-CHX and ISO-CHX natural circulation loops. The initial temperature of the loop fluid of all the loops is kept at 305 K to maintain uniformity in all the loops. At

the lower level of heat input, the temperature fluctuation is very high in all NCLs, and it never reaches a steady state throughout the operation of the loop. Whereas, at higher heat input, the fluctuation in temperature gets mitigated over time and reaches a steady-state eventually. Further, at the lower level of heat input, in all the loops, temperature fluctuation maintains the same pattern and amplitude throughout the operation of the loop. However, in the Heater-CHX loop, at 500 W and 1000 W heat fluxes, the amplitude of temperature fluctuation keeps increasing with time.

At a lower level of heat input, the temperature difference across source and sink will be very less, so the driving force will be less. This weak driving force strives to overcome all opposing forces in the loop, and if the driving force is greater than the opposing forces, the flow establishes. Since the driving force is very weak at lower heat input, at one point of time it fails to drive the fluid in the loop, and the velocity slides down. This tug-of-war in the loop continues or reaches a steady-state depending upon the imposed boundary conditions. Further, the time required to reach a steady state is also dictated by the quantum of heat input and boundary conditions at the source. The driving force will be very strong at higher heat due to stretched differential temperature across the source and sink. Higher the differential temperature higher will be the buoyancy effect and hence higher circulation rate [7]. It is very clearly visible in the graphs that as the temperature difference increase, the mass flow increases.

The amplitude of temperature fluctuation is very vigorous in the Heater-CHX loop, and it takes a longer duration to get mitigated at a higher level of input. Whereas, in the ISO-CHX loop, the amplitude of temperature fluctuation is insignificant and reaches a steady state at a shorter time duration. For given boundary conditions, the operating temperature of the loop fluid is highest in the Heater-CHX loop, and it is lowest in the case of the HHX-CHX loop.

Transient variation of mass flow rate

Figures 8a-e compare loop fluid mass flow rate (transient) in sCO₂ based NCLs configured with Heater-CHX, HHX-CHX and ISO-CHX, at source and sink, respectively, by varying the heat input at source keeping loop pressure fixed at 90 bar and sink temperature at 305K. Results are extracted at the centre of the right leg by considering the area-weighted average across the cross-section of the loop. The amplitude of mass flow fluctuation is very high at the lower level of heat input in all the loops and never reaches a stable state throughout the operation. However, at a higher level of heat input, the amplitude of mass flow fluctuation reduces considerably and eventually reaches a steady state.

At the lower level of heat input, in addition to mass flow fluctuation, the flow reversal occurs very frequently in all

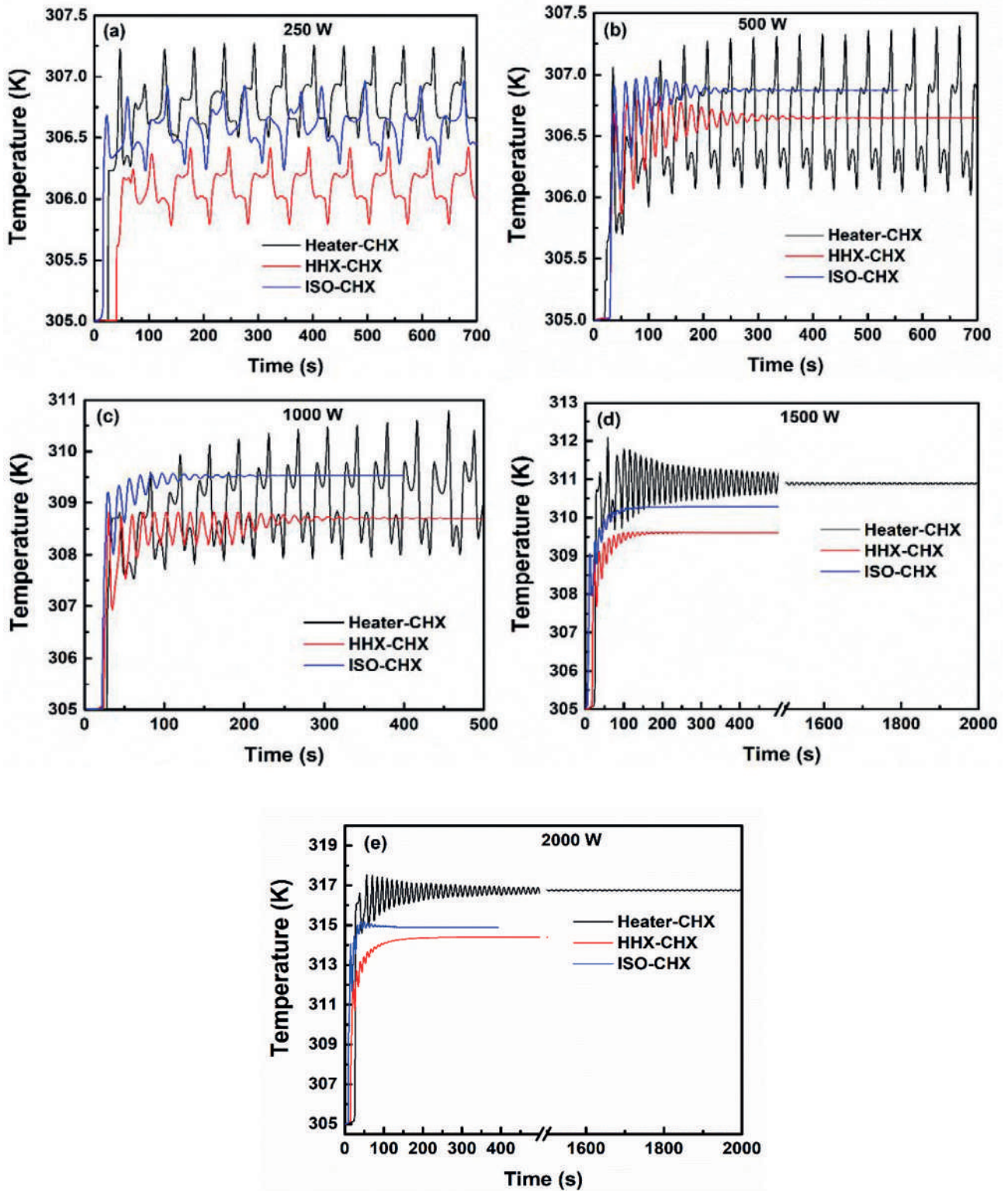


Figure 7. Variation of temperature at Heater-CHX, HHX-CHX and ISO-CHX for Supercritical CO₂ based natural circulation loop at different heat inputs of (a) 250 W, (b) 500 W, (c) 1000 W (d) 1500 W and (e) 2000 W.

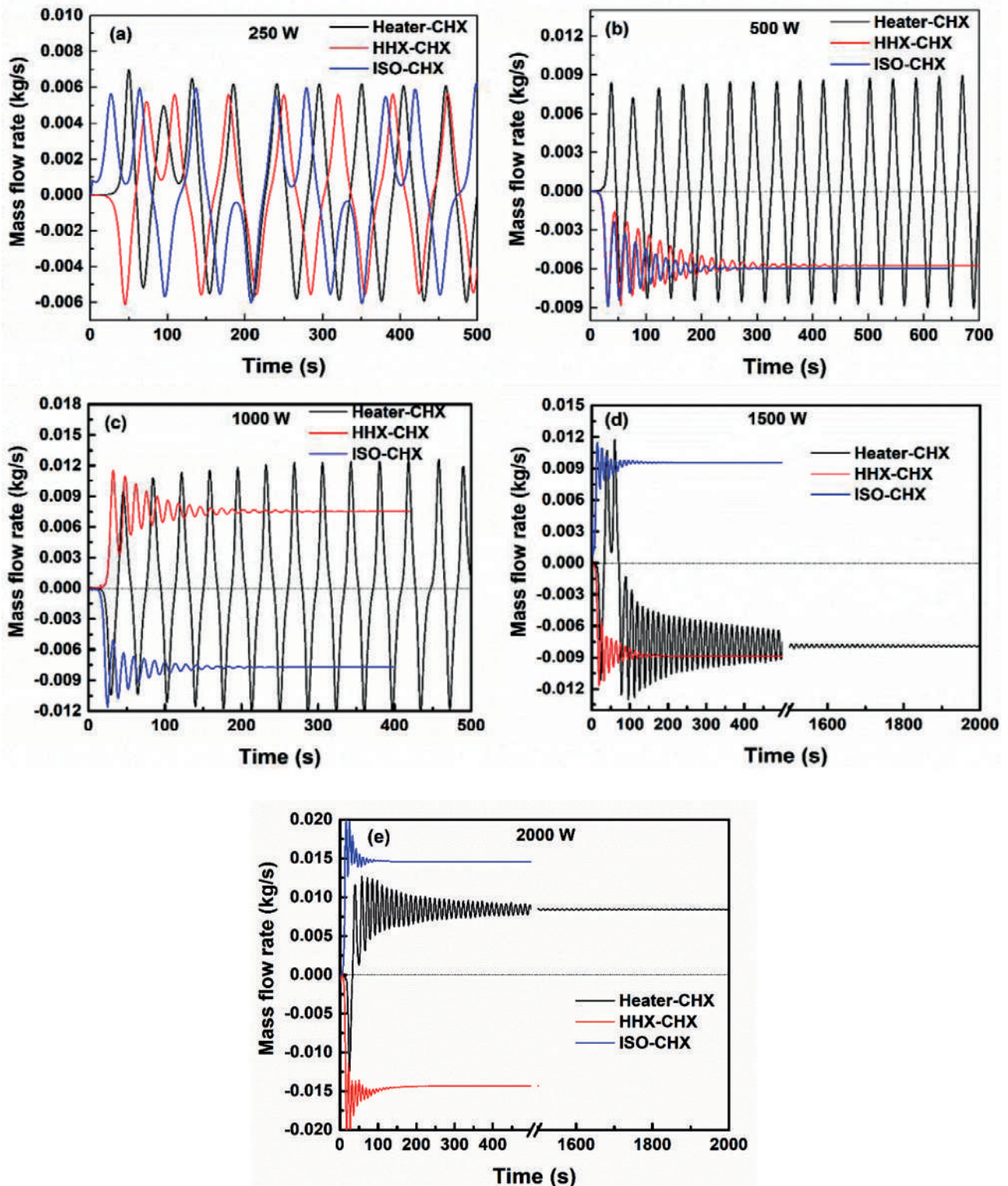


Figure 8. Variation of mass flow rate at Heater-CHX, HHX-CHX and ISO-CHX for Supercritical CO₂ based natural circulation loop at different heat inputs of (a) 250 W, (b) 500 W, (c) 1000 W (d) 1500 W and (e) 2000 W.

the loops. It is to be noted that, in the Heater-CHX loop, the mass flow reversal phenomenon is common at all levels of heat input, but its severity and duration of fluctuation reduce as heat input at the source increases. Whereas, no such reversal of mass flow is noticed in the other two loops except at the lowest level heat input, i.e., at 250 W.

At all heat input levels to the loop, the severity of mass flow oscillation is very high in the Heater-CHX loop compared to the other two loops. Further, it is to be noted that the mass flow rate, at steady state, is very low in the Heater-CHX loop compared to the other two loops at all levels of heat input to the loop. Further, at all levels of heat input, in the case of HHX-CHX and ISO-CHX loops, the magnitude of mass flow rate, at steady state, is virtually at the same level and is greater than the Heater-CHX loop.

It is evident from the graphs that in NCLs, the direction of mass flow is highly inconsistent and highly unpredictable. It is interesting to note that the direction of mass flow is independent of the boundary conditions on which NCLs are subjected and the quantum of heat input at the source. In the Heater-CHX loop, from 250 W to 1000 W of heat input, the mass flow reversal occurs frequently throughout the operation and never reaches a steady state. This phenomenon of flow reversals at the lower level of heat input may be due to the very low velocity of loop fluid. However, at 1500 W and 2000 W of heat input, the mass flow takes a definite direction after the initial reversal, but the direction is opposite to each other; however, it eventually reaches a steady-state condition. Similarly, in the case of the HHX-CHX loop, mass flow takes an anticlockwise direction at lower and higher levels of heat input, and at a moderate level of heat input, it takes a clockwise direction. Similarly, in the ISO-CHX loop, mass flow takes an anticlockwise direction at a lower level of heat input, mass flow takes an anticlockwise direction, and at a higher level of heat input, it changes to a clockwise direction. These unpredictable flow reversals and the direction of flow could be due to the bilaterally symmetrical geometry of NCLs in its vertical axis. Due to this geometrical symmetry of the loop, the resistance to flow in either direction will be identical, and hence the flow of loop fluid takes precedence and queue from the initial movement of the molecules at the heating section of the loop.

Transient Variation of Velocity

Figure 9 shows the velocity transient behaviour of loop fluid in Heater-CHX, HHX-CHX and ISOCHX natural circulation loops. The loop fluid magnitude of velocity is a direct function of the density difference between the source and the sink of the loop. Differential density in the loop is a function of the temperature difference between the source and sink, which will directly impact the mass flow rate of loop fluid in the loop. As the differential temperature increases across source and sink, the density difference between heating and cooling sections increases.

Impact on mass flow rate and velocity due to widening differential temperature is more pronounced in supercritical fluids as its viscosity is inherently lower than subcritical fluid. It is visible in the graph, i.e., at a lower level of heat input (250 W/308.5 K/306 K), the loop fluid average velocity is approximately in the range of 0.05 m/sec to 0.06 m/sec, and at a higher level of heat input (2000 W/320.75 K/313.5 K), it increases to a range of 0.19 m/sec to 0.24 m/sec, in the Heater-CHX, HHX-CHX and ISO-CHX loops respectively in ascending order. For a given boundary condition, among these three loops, the loop fluid velocity is very high in the ISO-CHX loop and lowest in the Heater-CHX loop.

During the initial stage of heat input, the loop experiences a very high fluctuation in velocity due to non-uniform heat distribution in the loop. The non-uniform distribution of heat creates an uneven accumulation of heat pockets at various locations in a system. These pockets suddenly release its accumulated heat when it moves to the cold region in the system. This sudden release of accumulated heat energy creates a huge density difference across the loop, leading to a very high-velocity fluctuation in the initial period. Over a period of time, once the system reaches the equilibrium state, i.e., when the quantity of heat addition and rejection is equal, and the driving force overcomes all the opposing forces in the system, the steady-state and unidirectional flow will establish. Similarly, with any heat input or pressure variation, the system will experience initial glitches and eventually settle down to a steady state.

At the lower rate of heat input, the oscillation of velocity in all loops is very high and never reaches a steady state. In all three loops, the magnitude of velocity oscillation is considerably higher at lower heat input, and it gradually decreases with the increase in the heat input. Further, the magnitude and frequency of velocity oscillation in the Heater-CHX are predominantly more at all heat input levels than HHX-CHX, and it is considerably subdued in the ISO-CHX loop.

In the ISO-CHX loop, the magnitude of velocity oscillation gets converges to a steady-state at a faster rate compared to the other two loops. Whereas in the Heater-CHX loop, the magnitude of velocity oscillation is very high, and it takes a considerably longer duration to get converge to a steady state compared to the other two loops. In all NCLs configurations, as the heat input increases at the source, the amplitude of velocity decreases, and it reaches to steady-state at a faster rate.

Effect of operating pressure

Figure 10 shows the transient behaviour of mass flow rate at various loop fluid pressure for all three loops, i.e., Heater-CHX, HHX-CHX and ISO-CHX loops. From the graphs, it can be inferred that the magnitude and frequency of mass flow oscillation decrease with an increase

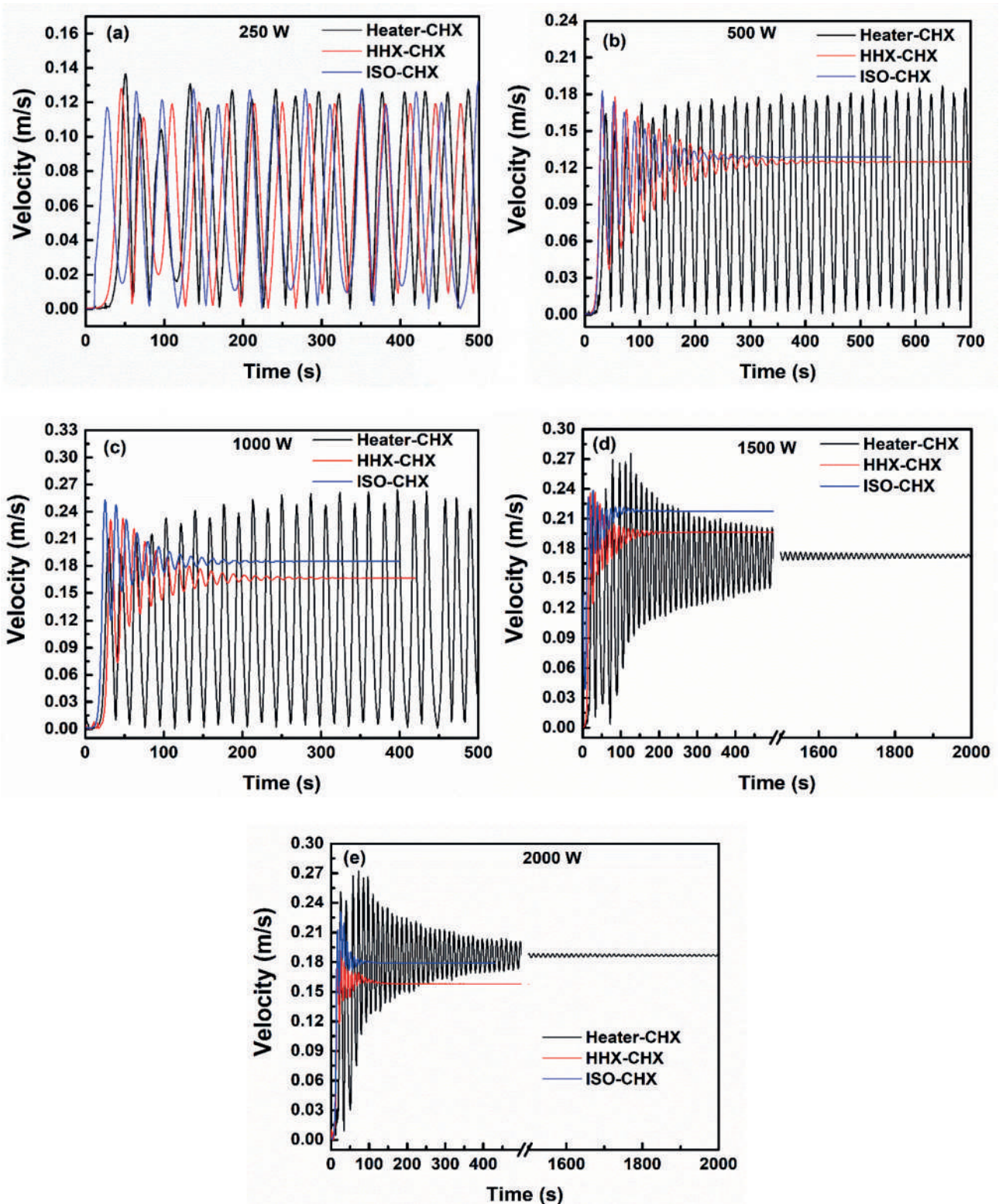


Figure 9. Variation of velocity for Heater-CHX, HHX-CHX and ISO-CHX for Supercritical CO₂ based natural circulation loop at different heat inputs of (a) 250 W, (b) 500 W, (c) 1000 W (d) 1500 W and (e) 2000 W.

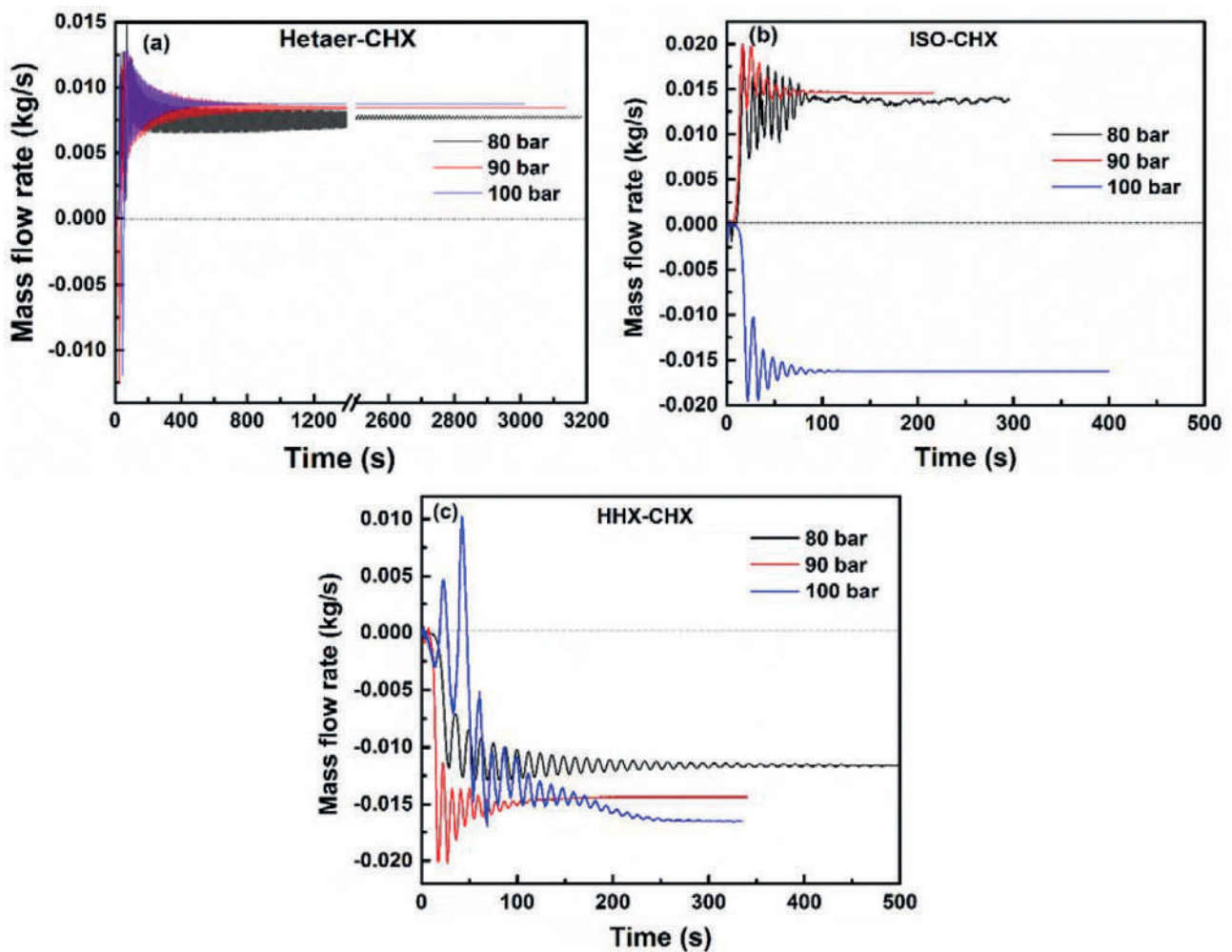


Figure 10. Effect of operating pressure (80 bar, 90 bar and 100 bar) for Supercritical CO₂ based natural circulation loop at 2000 W heat inputs for (a) Heater-CHX (b) HHX-CHX and (c) ISO-CHX.

in loop pressure for all three loops. It is very interesting to note that as the operating pressure of the sCO₂ increases, the time duration required to reach a steady-state of the system decreases, the same results are observed in the experimental study of Yadav et al. [29]. Further, the pressure has a significant effect on the mass flow rate in all three loops i.e., mass flow rate increases with an increase in the loop fluid pressure, the same phenomenon is observed in a CFD analysis of Archana et al. [31] on sCO₂ based NCL.

In general, the supercritical fluids attain a maximum density when it reaches its critical temperature and pressure. Around the critical region, the impact on the fluid density will be huge even for a slight variation in the temperature and pressure. The fluid keeps reaching its peak density and reverts very frequently, which induces density waves in the system. In a natural circulation system, these density waves will affect various operating parameters and create an imbalance among the natural driving force, frictional forces

and other forces. If the variation in density reaches a very high value, it leads to flow reversal in the loop.

In natural circulation systems, the driving force shall balance with the resistive force for the flow to get established. Appropriated agreement between the driving force and resistive force is the prerequisite for a stable state in the natural circulation loops. The resistive force is a function of friction factor, mass flow rate and average density along the loop. In compressible fluids, the average loop density increases with an increase in the loop pressure and it supplements the buoyancy effect in the system due to lower viscosity, which increases the mass flow rate. Further, with the increase in density and hence the mass flow rate, the resistive forces in the loop increases (i.e., viscous dissipation and friction between wall and fluid). The resistive force thus increased counters the buoyancy force and suppresses the mass flow rate in the loop. Again, the buoyancy force strives to overcome the resistive force, and this tug of war will continue between these two forces until there is a

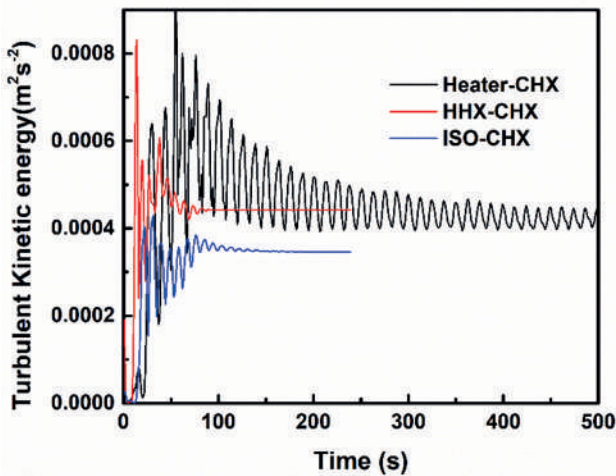


Figure 11. Turbulence Kinetic Energy for Supercritical CO₂ based Heater-CHX, HHXCHX and ISO-CHX natural circulation loop.

balance between them, and it is the root cause for the instability/oscillation in the natural circulation loops [35]. This concept is visible from the following graphs, i.e., increase in mass flow rate with increase in loop pressure.

The flow instability in the Heater-CHX loop is very high compared to the other two loops, and also it takes a longer time to reach a steady state at lower pressure compared to higher pressure. It may be due to the direct impact of heat fluxes on the loop fluid at the source of the loop. In the Heater-CHX loop, at lower pressure, the mass flow is unidirectional, whereas at higher pressure, as soon as the loop is exposed to heat energy at the source, for a small period of time in the initial stage, the mass flow takes a bidirectional path and after that, it follows a unidirectional path.

The influence of operating pressure on the loop fluid mass flow oscillation is moderate in the HHX-CHX loop compared to the other two loops. At all operating pressure of the loop fluid, in the Heater-CHX loop, the mass flow takes a clockwise direction, and contrary to this occurrence, in the HHX-CHX loop, it takes an anticlockwise direction.

The influence of the operating pressure of the loop fluid on the mass flow oscillation is very mild in the ISO-CHX loop compared to the other two loops. This may be due to the impulsive response of the isothermal wall for any change in heat input at the source, as temperature distribution is uniform throughout the heating section of the loop. This uniform temperature distribution effectively dampens the mass flow fluctuations faster, leading to a faster rate of stabilization of the system. Further in this loop, as the loop fluid's operating pressure increases, the mass flow changes its flow direction from clockwise to anticlockwise direction. It is unique in the ISO-CHX loop compared to the other two loops under study.

Variation of turbulence kinetic energy

Figure 11 depicts the profile of turbulence kinetic energy variation in all three NCL configurations at 90 bar pressures for the heat input of 2000 W heat fluxes at source in Heater-CHX loop and the temperature of 320.75 K at the hot heat exchanger inlet of HHX-CHX loop and the uniform temperature of 313.50 K at the Isothermal wall of ISO-CHX loop. Turbulent flow is a property of the fluid flow but not a fluid physical characteristic. Velocity, pressure and other parameters irregular fluctuations cause turbulent flow in the loop.

Turbulent flow is characterized by fluctuating velocity fields in the flow region, which is highly chaotic as both velocity and pressure vary randomly with time. Random quantities are generally four-dimensional functions of space-time. Turbulence kinetic energy is the average kinetic energy per unit mass which is associated with oscillatory fluid flow. The turbulent energy generated in the flow is proportional to shear stresses, i.e., frictional and buoyant forces. In general, Reynolds averaged equations (RNG), i.e., k - ϵ equations of turbulence models, evaluate the turbulent energy in the flow field. The ANSYS FLUENT standard k - ϵ of turbulence is considered in the present study to compare turbulence kinetic energy profile in various NCLs as it ensures reasonably fair accuracy for a wide range of turbulent flows. It is to be noted from the temperature profiles of NCLs that, for given boundary conditions, the operating temperature of the loop fluid is highest in the Heater-CHX loop compared to other loops. Flow turbulence is a function of temperature, and hence higher the temperature indicates higher turbulence in the loop. Further, higher the turbulent energy in the fluid flow field indicates a higher heat transfer rate. Exceptionally excellent Turbulent kinetic energy in the Heater-CHX loop exhibits a better heat transport property than other loops. Further, a higher Nusselt number in the Heater-CHX loop also supplements its better heat transport property.

Nusselt number

Figure 12 shows the effect of heat input on the Nusselt number for all three NCLs, i.e., Heater-CHX, HHXCHX and ISO-CHX loops. The Nusselt number, a non-dimensional form of heat transfer coefficient, is a function of Reynolds number and Prandtl number (Pr), i.e., in the loop, the Nusselt number increases with an increase in Reynolds number. The magnitude of the Reynolds number increases with an increase in the loop differential temperature, which indicates the increase in turbulence and hence the higher rate of heat transfer. Nusselt number in the Heater-CHX loop is very high compared to the other two configurations at all levels of heat input, and it keeps on increasing with an increase in the heat input at source in all NCLs. HHX-CHX NCL configuration demonstrated the least level of Nusselt number among the cluster of NCLs considered for analysis. The performance of ideal

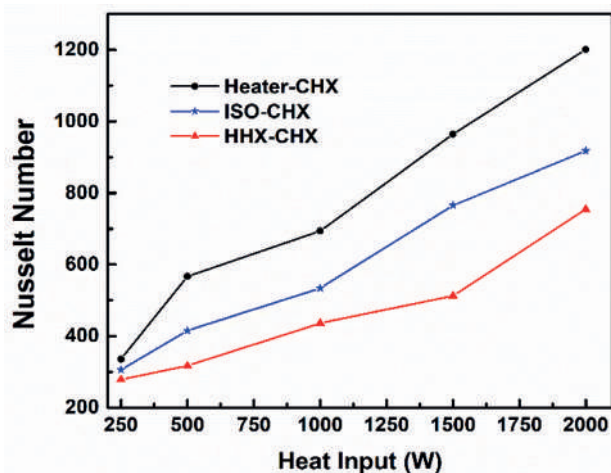


Figure 12. Variation of Nusselt number with heat input for CO₂ based Heater-CHX, HHXCHX and ISO-CHX natural circulation loop.

NCL, i.e., ISO-CHX loop, lies in between the two practical NCLs.

CONCLUSION

Three-dimensional CFD simulations were conducted on three different combinations of source and sink in sCO₂ based square NCLs to study the influence of change in boundary condition and operating pressures on transient and instability behaviour of loop reveals the following:

1. NCLs show instability in the form of oscillation or both oscillation, flow reversal and the time required for these instabilities to attain a steady-state depends on the nature of the chosen boundary condition or the quantum of heat input applied at the source.
2. The loop fluid mass flow rate, temperature and velocity oscillation in the Heater-CHX loop are very high compared to the ISO-CHX loop. This difference in the behaviour of loops is inherent because the heat transfer rate is fixed and independent of loop fluid temperature in heater, but in other cases, the heat transfer rate depends on loop fluid temperature. Stability performance of HHX-CHX loop sets in these two loops.
3. In the ISO-CHX loop, the mass flow and temperature instabilities stabilized faster than Heater-CHX and HHX-CHX loops, as its response at source is instantaneous due to constant temperature throughout the heating section.
4. For given boundary conditions, the operating temperature of the loop fluid is highest in the Heater-CHX loop and it is lowest in the HHX-CHX loop.
5. In all configurations of NCLs considered in the present study, the mass flow rate increases with an increase in loop fluid operating pressure, whereas flow instabilities

decrease with an increase in loop fluid operating pressure. It is found that as the operating pressure of the sCO₂ increases, the time duration required to reach a steady-state of the system decreases.

6. At all heat input levels at the source, the average mass flow rate is lower, and the time taken for the velocity oscillations to dampen is very high in the Heater-CHX loop compared to the other two loops. Whereas the amplitude of flow oscillation is very mild and velocity oscillations convergence at a shorter time duration in the ISO-CHX loop compared to the other two loops.
7. In all configurations of NCL, at lower heat input, the loop fluid flow takes a bidirectional path at regular intervals. However, it follows a unidirectional path at higher heat input except for inconsequential initial glitches in the Heater-CHX loop. Further, the direction of flow is highly inconsistent and extremely unpredictable in all configurations of NCL considered. The direction of mass flow is independent of the boundary conditions and quantum of heat input.
8. Nusselt number in the Heater-CHX loop is very high compared to HHX-CHX and ISO-CHX loops because of its high turbulent kinetic energy and it leads to better heat transport property in the case Heater-CHX loop.

ACKNOWLEDGMENT

The present experimental work is supported under a sponsored project by Science and Engineering Research Board, Department of Science and Technology, Government of India (SB/FTP/ETA-443/2013). The gratefully acknowledged financial support offered by DST-SERB.

AUTHORSHIP CONTRIBUTIONS

Authors equally contributed to this work.

DATA AVAILABILITY STATEMENT

The authors confirm that the data that supports the findings of this study are available within the article. Raw data that support the finding of this study are available from the corresponding author, upon reasonable request.

CONFLICT OF INTEREST

The author declared no potential conflicts of interest with respect to the research, authorship, and/or publication of this article.

ETHICS

There are no ethical issues with the publication of this manuscript.

NOMENCLATURE

A	Area, m^2
C_p	Specific heat, $J/kg - K$
d	Particle diameter, m^2
g	Acceleration due to gravity, m/s^2
h	Enthalpy, J/kg
m	Mass flow rate, kg/s .
p	Pressure, Pa
pr	Prandtl number, $pr = \frac{\mu C_p}{\lambda}$
Pr_T	Turbulent Prandtl number
Q	Heat input, W
Re	Reynolds number, $Re = \frac{\rho v d}{\mu}$
sCO_2	Supercritical carbon dioxide
sCO_2NCL	Supercritical carbon dioxide based NCL
T	Temperature, K
t	Time, s
u	Velocity in X-direction, m/s
v	Velocity in Y-direction, m/s
w	Velocity in Z-direction, m/s

Greek symbols

\bar{h}	Heat transfer coefficient, W/m^2K
β	Volumetric expansion coefficient, $1/K$
κ	Turbulent kinetic energy, m^2/s^3
λ	Thermal conductivity, $W/m.K$
μ	Viscosity, $Pa. s$
μ_T	Turbulent Viscosity, $C_\mu \rho \frac{\kappa^2}{\epsilon}$
ϵ	Turbulent Kinetic energy dissipation rate, m^2/s^3
G	Rate of generation of turbulent kinetic energy, $kg/m.s^2$

Subscripts

r	radial direction
ss	Steady state
x	local, value of axial direction

REFERENCES

- [1] Chen PC, Lin WK. The application of capillary pumped loop for cooling of electronic components. *Appl Therm Eng* 2001;21:1739–1754. [CrossRef]
- [2] Kumar KK, Gopal MR. Carbon dioxide as a secondary fluid in natural circulation loops. *Proc Inst Mech Eng E J Process Mech Eng* 2009;223:189–194. [CrossRef]
- [3] Mertol A, Greif R, Zvirin Y. Two dimensional analysis of transient flow and heat transfer in a natural circulation loop. *Wärme-und Stoffübertragung* 1984;18:89–98. [CrossRef]
- [4] Lifshitz S, Zvirin Y. Transient heat and mass transfer in a natural circulation loop. *Wärme-und Stoffübertragung* 1993;28:371–380. [CrossRef]
- [5] Acosta R, Sen M, Ramos E. Single-phase natural circulation in a tilted square loop. *Wärme-und Stoffübertragung* 1987;21:269–275. [CrossRef]
- [6] Lin JF, Chiu S, Ho CJ. Conjugate heat transfer simulation of a rectangular natural circulation loop. *Heat Mass Transf* 2008;45:167. [CrossRef]
- [7] Cheng H, Lei H, Dai C. Heat transfer of a single-phase natural circulation loop with heating and cooling fluids. *Energy Procedia* 2017;142:3926–3931. [CrossRef]
- [8] Vijayan PK, Patil A, Pikhwal D, Saha D, Raj VV. An assessment of pressure drop and void fraction correlations with data from two-phase natural circulation loops. *Heat Mass Transf* 2000;36:541–548. [CrossRef]
- [9] Yadav AK, Maddali RG, Bhattacharyya S. On the suitability of carbon dioxide in forced circulation-type secondary loops. *Int J Low-Carbon Technol* 2014;9:85–90. [CrossRef]
- [10] Blackburn JM, Long DP, Cabanas A, Watkins JJ. Deposition of conformal copper and nickel films from supercritical carbon dioxide. *Science* 2001;294:141–145. [CrossRef]
- [11] Chen L, Zhang XR. Experiments on natural convective solar thermal achieved by supercritical CO_2 /dimethyl ether mixture fluid. *J Sol Energy Eng* 2014;136. [CrossRef]
- [12] Dimmick G, Chatoorgoon H, Khartabil V, Duffey R. Natural-convection studies for advanced Candu reactor concepts. *Nucl Eng Des* 2002;215:27–38. [CrossRef]
- [13] Yamaguchi H, Zhang XR, Fujima K. Basic study on new cryogenic refrigeration using CO_2 solid-gas two-phase flow. *Int J Refrig* 2008;31:404–410. [CrossRef]
- [14] Lee HS, Kim HJ, Yoon JI, Choi KH, Son CH. The cooling heat transfer characteristics of the supercritical CO_2 in a micro-fin tube. *Heat Mass Transf* 2013;49:173–184. [CrossRef]
- [15] Neksa P, Rekestad H, Zakeri GR, Schiefloe PA. CO_2 -heat pump water heater: characteristics, system design and experimental results. *Int J Refrig* 1998;21:172–179. [CrossRef]
- [16] Bettini R, Bertolini G, Frigo E, Rossi A, Casini I, Pasquali I, et al. Interaction of pharmaceutical hydrates with supercritical CO_2 . *J Therm Anal Calorim* 2004;77:625–638. [CrossRef]
- [17] Kim YM, Sohn JL, Yoon ES. Supercritical CO_2 Rankine cycles for waste heat recovery from a gas turbine. *Energy* 2017;118:893–905. [CrossRef]
- [18] Yadav AK, Ramgopal M, Bhattacharyya S. CO_2 based natural circulation loops: new correlations for friction and heat transfer. *Int J Heat Mass Transfer* 2012;55:4621–4630. [CrossRef]
- [19] Yadav AK, Bhattacharyya S, Ramgopal M. Optimum operating conditions for subcritical/supercritical

- fluid-based natural circulation loops. *J Heat Transf* 2016;138. [\[CrossRef\]](#)
- [20] Thippeswamy LR, Yadav AK. Heat transfer enhancement using CO₂ in a natural circulation loop. *Sci Rep* 2020;10:1–10. [\[CrossRef\]](#)
- [21] Hahne EW. Natural convection heat transfer through an enclosed horizontal layer of supercritical carbon dioxide. *Wärme-und Stoffübertragung* 1968;1:190–196. [\[CrossRef\]](#)
- [22] Zhang XR, Chen L, Yamaguchi H. Natural convective flow and heat transfer of supercritical CO₂ in a rectangular circulation loop. *Int J Heat Mass Transf* 2010;53:4112–4122. [\[CrossRef\]](#)
- [23] Misale M, Ruffino P, Frogheri M. The influence of the wall thermal capacity and axial conduction over a single-phase natural circulation loop: 2-D numerical study. *Heat and Mass Transf* 2000;36:533–539. [\[CrossRef\]](#)
- [24] Janardhana Reddy G, Basha H, Venkata Narayanan N. Transient natural convection heat transfer to CO₂ in the supercritical region. *J Heat Transfer* 2018;140:092502. [\[CrossRef\]](#)
- [25] Chen L, Zhang XR. Simulation of heat transfer and system behaviour in a supercritical CO₂ based thermosyphon: effect of pipe diameter. *J Heat Transfer* 2011;133:122505. [\[CrossRef\]](#)
- [26] Sadhu S, Ramgopal M, Bhattacharyya S. Steady-state analysis of a high-temperature natural circulation loop based on water-cooled supercritical CO₂. *J Heat Transfer* 2018;140:062502. [\[CrossRef\]](#)
- [27] Liu G, Huang Y, Wang J, Leung LH. Heat transfer of supercritical carbon dioxide flowing in a rectangular circulation loop. *Appl Therm Eng* 2016;98:39–48. [\[CrossRef\]](#)
- [28] Deng B, Chen L, Zhang X, Jin L. The flow transition characteristics of supercritical CO₂ based closed natural circulation loop (ncl) system. *Ann Nucl Energy* 2019;132: 134–138. [\[CrossRef\]](#)
- [29] Yadav AK, Ramgopal M, Bhattacharyya S. Transient analysis of subcritical/supercritical carbon dioxide-based natural circulation loop with end heat exchangers: Experimental study. *Heat Mass Transf* 2017;53:2951–2960. [\[CrossRef\]](#)
- [30] Yadav AK, Ramgopal M, Bhattacharyya S. Transient analysis of subcritical/supercritical carbon dioxide-based natural circulation loops with end heat exchangers: Numerical studies. *Int J Heat Mass Transfer* 2014;79:24–33. [\[CrossRef\]](#)
- [31] Archana V, Vaidya A, Vijayan P. Effect of pressure on steady-state and heat transfer characteristics in supercritical CO₂ natural circulation loop. *Procedia Eng* 2015;127:636–644. [\[CrossRef\]](#)
- [32] Karakurt AS, Bashan V, Ust Y. Comparative maximum power density analysis of a supercritical CO₂ Brayton power cycle. *J Therm Eng* 2020;6:50–57. [\[CrossRef\]](#)
- [33] Wang CC, Zhu CX, Tang YC. Performance and flow distribution of the plate heat exchanger with supercritical fluid of carbon dioxide. *J Therm Eng* 2015;1:143–151.
- [34] Chen K. On the oscillatory instability of closed-loop thermosyphons. *J Heat Transf* 1985;107:826–832. [\[CrossRef\]](#)
- [35] Keller JB. Periodic oscillations in a model of thermal convection. *J Fluid Mech* 1966;26:599–606. [\[CrossRef\]](#)
- [36] Welander P. On the oscillatory instability of a differentially heated fluid loop. *J Fluid Mech* 1967;29:17–30. [\[CrossRef\]](#)
- [37] Schuster C, Ellinger A, Knorr J. Analysis of flow instabilities at the natural circulation loop Danton with regard to non-linear effects. *Heat Mass Transf* 2000;36:557–565. [\[CrossRef\]](#)
- [38] Vijayan PK, Sharma M, Pikhwal D, Saha D, Sinha R. A comparative study of single-phase, two-phase, and supercritical natural circulation in a rectangular loop. *J Eng Gas Turbines Power* 2010;132:102913. [\[CrossRef\]](#)
- [39] Stern C, Greif R. Measurements in a natural convection loop. *Wärme-und Stoffübertragung* 1987;21: 277–282. [\[CrossRef\]](#)
- [40] Chen L, Zhang XR, Yamaguchi H, Liu ZSS. Effect of heat transfer on the instabilities and transitions of supercritical CO₂ flow in a natural circulation loop. *Int J Heat Mass Transf* 2010;53:4101–4111. [\[CrossRef\]](#)
- [41] Creveling H, De Paz J, Baladi J, Schoenhals R. Stability characteristics of a single-phase free convection loop. *J Fluid Mech* 1975;67:65–84. [\[CrossRef\]](#)
- [42] Kapitza M. The effect of the location of nucleation sites on the thermal-hydraulic stability of a short-tube natural circulation loop. *J Eng Gas Turbines Power* 2012; 134:062901. [\[CrossRef\]](#)
- [43] Misale M. Experimental study on the influence of power steps on the thermohydraulic behaviour of a natural circulation loop. *Int J Heat Mass Transf* 2016;99:782–791. [\[CrossRef\]](#)
- [44] Furuya M, Inada F, Yasuo A. Inlet throttling effect on the boiling two-phase flow stability in a natural circulation loop with a chimney. *Heat Mass Transf* 2001;37:111–115. [\[CrossRef\]](#)
- [45] Yadav AK, Ramgopal M, Bhattacharyya S. Effect of tilt angle on subcritical/supercritical carbon dioxide-based natural circulation loop with isothermal source and sink. *J Therm Sci Eng Appl* 2016;8:011007. [\[CrossRef\]](#)
- [46] Manero E, Sen M, Ramos E. Two-phase natural circulation in a toroidal loop. *Wärmeund Stoffübertragung* 1987;21:41–49. [\[CrossRef\]](#)
- [47] Yadav AK, Ramgopal M, Bhattacharyya S. CFD analysis of a CO₂ based natural circulation loop with

- end heat exchangers. *Appl Therm Eng* 2012;36:288–295. [\[CrossRef\]](#)
- [48] Zvirin Y. Throughflow effects on the transient and stability characteristics of a thermosyphon. *Wärme- und Stoffübertragung* 1985;19:113–120. [\[CrossRef\]](#)
- [49] Cammarata L, Fichera A, Guglielmino I, Pagano A. On the effect of gravity on the bifurcation of rectangular closed-loop thermosyphon. *Heat Mass Transf* 2004; 40:801–808. [\[CrossRef\]](#)
- [50] Cammarata L, Fichera A, Pagano A. Stability maps for rectangular circulation loops. *Appl Therm Eng* 2003;23:965–977. [\[CrossRef\]](#)
- [51] Jiang Y, Shoji M. Spatial and temporal stabilities of flow in a natural circulation loop: influences of thermal boundary condition. *J Heat Transf* 2003;125:612–623. [\[CrossRef\]](#)
- [52] Vijayan PK, Sharma M, Saha D. Steady-state and stability characteristics of single-phase natural circulation in a rectangular loop with different heater and cooler orientations. *Exp Therm Fluid Sci* 2007;31:925–945. [\[CrossRef\]](#)
- [53] Chen L, Zhang XR, Jiang B. Effects of heater orientations on the natural circulation and heat transfer in a supercritical CO₂ rectangular loop. *J Heat Transfer* 2014;136:052501.
- [54] Wahidi T, Chandavar RA, Yadav AK. Stability enhancement of supercritical CO₂ based natural circulation loop using a modified tesla valve. *J Supercrit Fluids* 2020;166:105020. [\[CrossRef\]](#)
- [55] Wahidi T, Yadav AK. Instability mitigation by integrating twin tesla type valves in supercritical carbon dioxide-based natural circulation loop. *Appl Therm Eng* 2021;182:116087. [\[CrossRef\]](#)
- [56] Sharma M, Vijayan P, Pilkhwal D, Saha D, Sinha R. Linear and nonlinear stability analysis of a supercritical natural circulation loop. *J Eng Gas Turbines Power* 2010;132:102904. [\[CrossRef\]](#)
- [57] Seyyedi S, Sahebi N, Dogonchi A, Hashemi-Tilehnoee M. Numerical and experimental analysis of a rectangular single-phase natural circulation loop with asymmetric heater position. *Int J Heat Mass Transf* 2019;130:1343–1357. [\[CrossRef\]](#)
- [58] Manthey R, Schuster C, Lippmann W, Hurtado A. Effect of throttling on the two-phase flow stability in an open natural circulation system. *Heat and Mass Transf* 2020;56:37–52. [\[CrossRef\]](#)
- [59] Jiang S, Wu X, Zhang Y, Jia H. Thermal hydraulic modelling of a natural circulation loop. *Heat Mass Transf* 2001;37:387–395. [\[CrossRef\]](#)
- [60] Rao NM, Maiti B, Das PK. Stability behaviour of a natural circulation loop with end heat exchangers. *J Heat Transf* 2005;127:749–759. [\[CrossRef\]](#)
- [61] Thimmaiah S, Wahidi T, Yadav AK, Mahalingam A. Comparative computational appraisal of supercritical CO₂ based natural circulation loop: effect of heat-exchanger and isothermal wall. *J Therm Anal Calorim* 2020;141:2219–2229. [\[CrossRef\]](#)
- [62] Roache PJ, Ghia KN, White FM. Editorial policy statement on the control of numerical accuracy. *J Fluids Eng* 1986;108:2. [\[CrossRef\]](#)
- [63] Lisboa PF, Fernandes J, Simões PC, Mota JP, Saadjan E. Computational-fluid dynamics study of a kenics static mixer as a heat exchanger for supercritical carbon dioxide. *J Supercrit Fluids* 2010;55:107. [\[CrossRef\]](#)
- [64] NIST Standard Reference Database 23: Refprop version 9.0., Reference Fluid Thermodynamic and Transport Properties, Standard Reference Data Program Software, National Institute of Standards and Technology, Gaithersburg, MD 2013.
- [65] Swapnalee BT, Vijayan PK, Sharma M, Pilkhwal DS. Steady-state flow and static instability of supercritical natural circulation loops. *Nucl Eng Des* 2012;245:99–112. [\[CrossRef\]](#)